

Laser collimation of a chromium beam

R. E. Scholten,* R. Gupta, J. J. McClelland, and R. J. Celotta

Electron Physics Group, National Institute of Standards and Technology, Gaithersburg MD 20899

USA

M. S. Levenson and M. G. Vangel

Statistical Engineering Division, National Institute of Standards and Technology, Gaithersburg

MD 20899 USA

(October 16, 1996)

Abstract

We have studied laser collimation of a chromium atomic beam using a transverse polarization gradient cooling scheme. We present detailed measurements of the angular distribution of atoms on the beam axis, over a broad range of laser intensities and detunings including those which produce significant excitation, and observe collimation angles as small as 0.16 ± 0.01 mrad (50% quantile). We compare our results with existing calculations based on assumptions of steady-state conditions and low excited-state population.

I. INTRODUCTION

Collimated atomic beams play an important role in many applications of current interest, from atom interferometers [1] and atomic clocks [2] to collision studies [3] and direct-write nanofabrication [4]. While collimation can be achieved in a very straightforward way using nozzles and/or collimating apertures [5,6], these approaches generally result in a great loss of flux. Recently, laser cooling techniques, which utilize dissipative forces to increase the brightness of atomic beams, have arisen as an alternative that provides high degrees of collimation without significant loss of flux [7–9].

We report here results on laser collimation of a thermal chromium atomic beam using one-dimensional transverse sub-Doppler polarization-gradient laser cooling. We have measured angular distributions of atoms on the beam axis for a range of laser intensities and detunings. We have also determined the conditions under which a minimum angular spread is obtained within the constraints of our experimental configuration. Many of the measurements are made under conditions of high excited-state fraction and non-steady-state conditions, so our data cover a new, relatively unexplored area. As a result, there is no theoretical work available for direct comparison. We compare our results with theoretical calculations based on assumptions of low excited-state fraction and steady-state conditions, in order to contrast this work with other laser cooling studies.

Background

Since the first experiments on cooling free atoms with near-resonant laser light [10], many cooling mechanisms have been identified, including Doppler-limited, sub-Doppler and sub-recoil cooling [11]. These techniques have been applied in one, two and three dimensions, to slow and trap atoms and to transversely cool and therefore collimate and brighten an atomic beam.

The fundamentals of laser cooling have been thoroughly described by several authors

[11]. In the simplest scheme, atoms are cooled in a region of counter-propagating laser beams, sometimes referred to as optical molasses, where the lasers are detuned below the atomic resonance. Due to the Doppler shift, it is more likely that atoms absorb light, and hence momentum, from the laser beam that is propagating opposite to their own motion.

Enhanced cooling can be obtained by employing polarization gradients in the laser field [12]. In particular, the (*lin* \perp *lin*) configuration uses two counter-propagating lasers with orthogonal linear polarizations to create a superposition with continually varying polarization. Atoms with the appropriate transitions (angular momentum $J \rightarrow J + 1$, $J \neq 0$) experience laser forces which depend on the polarization, such that motion against the polarization gradients results in additional velocity-dependent forces and the associated cooling effects.

In recent years, the understanding of polarization-gradient laser cooling has evolved to the point where it appears to follow near-universal behavior if one concentrates on the limit of low excited-state fraction and assumes that steady-state conditions have been attained. These circumstances can be found, for example, in a three-dimensional atom trap, or when slow atoms are cooled in one dimension over a long interaction distance.

Given these conditions, the temperature of the cooled atoms, (or equivalently the RMS velocity spread, or the average kinetic energy E_k) is found to depend (for a given $J \rightarrow J + 1$ transition) only on the light shift potential U_0 [12–16]. This quantity, which incorporates the essential laser parameters of intensity and detuning, represents in a single number the effective depths of an array of light-shift potentials associated with the different magnetic substates of the atom and their differing interactions with the varying polarization state of the laser. In terms of the laser parameters, U_0 is given by [16]

$$U_0 = \hbar|\Delta|\frac{\Omega^2}{4\Delta^2 + \Gamma^2}. \quad (1)$$

Here Γ is the linewidth of the transition, Δ is the laser detuning with respect to the atomic transition frequency, and Ω is the Rabi frequency for the strongest magnetic sublevel transition, i.e., for $|M| = J \rightarrow |M| = J + 1$. The Rabi frequency is given by $\Omega^2 = \frac{1}{2}\Gamma^2(I/I_0)$, where I is the intensity of the laser field, and I_0 is the saturation intensity for the transition

[17].

When comparing laser cooling for different atoms, it is useful to scale the light shift and the average kinetic energy E_k by the recoil energy, $E_r \equiv \hbar^2 k^2 / 2M$, of an atom with mass M absorbing or emitting a photon of momentum $\hbar k$ [18]. With this scaling, the near-universal behavior becomes apparent. The average kinetic energy of the atoms initially falls rapidly with U_0 , reaching a minimum when the light shift reaches a value around $U_0 = 50E_r$ [14,16]. Typical experimental values of this minimum average kinetic energy in 3-D experiments are $E_k(\text{min}) = 32E_r$ for rubidium ($J = 3 \rightarrow 4$) [18], $26E_r$ for cesium ($J = 4 \rightarrow 5$) [19] and $22E_r$ for sodium ($J = 2 \rightarrow 3$) [17]. From the minimum, the average kinetic energy increases approximately linearly as a function of light shift with a slope of about 0.14 in one dimension [14–16,20] and 0.35 in three dimensions [18,19] for all atoms investigated so far.

This work

While a fairly good understanding has evolved of laser cooling in low-excitation, steady-state conditions, less is known about the situation examined by the current study. In our work, the major emphasis is the attainment of a high degree of collimation in a thermal atom beam using laser cooling over a necessarily limited interaction region. Because of the relatively fast atomic speeds and short interaction region, steady-state conditions do not exist over the full range of parameters investigated. Despite this, we observe collimations that are not very different from those expected in a steady-state situation. The apparent reason for this is our use of higher laser intensities; stronger cooling appears to compensate for the lack of complete steady-state conditions. Though this improves the collimation of the atom beam, it brings the conditions of our experiments further from the regime of well-understood laser cooling, which is restricted to low excitation fractions.

Our experiments measure the angular distribution of atoms in a chromium atomic beam after interacting with a polarization gradient laser cooling process. The angular distributions we present are spatially resolved; we observe only those atoms passing through a point in

the center of the beam and measure the probability that an atomic trajectory has a certain angle relative to the beam axis. We have concentrated on two goals: (i) obtaining the highest degree of collimation within the constraints of our apparatus, and (ii) gaining further insight into laser cooling at high excited state fraction and non-steady-state conditions.

In addition to measuring and presenting the full angular distributions, we have also derived 50% and 90% angular quantiles. These are defined as the full angular width centered about zero that contains 50% (or 90%) of the integrated angular distribution. Though these angular measures depart from the more conventional full width at half maximum or RMS spread, we find them to be a convenient and unbiased way to represent the width of a distribution whose functional form is completely unspecified. In addition, the quantile is the true number of interest where the ultimate goal is to collimate a beam so that as many atoms as possible pass through an aperture.

In searching for the highest degree of collimation, we concentrated on finding the laser configuration that minimized both the 50% and 90% quantiles. Our smallest quantiles were obtained with a cooling laser having a Gaussian profile along the atom beam axis. For a $1/e^2$ full width of 23 ± 1 mm, we found that 90% of the beam was cooled into 0.61 ± 0.02 mrad (full angle) and 50% into 0.16 ± 0.01 mrad, using a laser power of 40 mW and a detuning of $-\Gamma$ [21].

Although a Gaussian laser beam gave narrower collimation angles, we chose to truncate the beam profile, to more closely approximate a uniform illumination, for our studies of collimation as a function of laser parameters. This allowed us to establish a well-defined interaction length for the atoms, and also to perform experiments under more nearly constant-intensity conditions. This eliminated the possibility of any adiabatic cooling effects in the gradually decreasing intensity of a Gaussian tail [22].

II. ANGLE AND VELOCITY DISTRIBUTIONS

This experiment, which produces and measures the collimation of an atomic beam, is, in some ways, very similar to experiments that study transverse laser cooling. However, it is important to recognize that angular distribution measurements (which we report) cannot directly provide the transverse velocity distribution (frequently obtained in transverse cooling experiments) without making some assumptions. Two problems prevent us from establishing this relationship: (1) we do not know *a priori* the shape, or functional form, of the transverse velocity distribution after cooling, and (2) there is an unknown degree of correlation between longitudinal and transverse velocities. Characterizations of, or assumptions about, both of these effects are required for a deconvolution of the transverse velocity distribution from the beam angular distribution and the known longitudinal velocity distribution.

The functional form of the transverse velocity distribution is undetermined because of the departure from the low-excited-state limit. While for low excited-state fraction the transverse velocity distribution is expected to be Gaussian in shape [16], a high excited-state fraction has been seen theoretically to result in a distinctly non-Gaussian distribution, with a narrow central feature and broad wings [23,24].

The correlation between transverse and longitudinal velocities is unknown because we generally do not have steady-state conditions. If the steady state is fully reached, it is reasonable to assume that the transverse velocities are fully thermalized and no correlation remains between the longitudinal and transverse velocities. If steady-state is not reached, however, we must allow for two possible sources of correlation. A correlation could occur because of our limited interaction distance, which can result in longitudinally faster atoms interacting with the laser for shorter times and thus being cooled less. Also, it could be a remnant of the correlation present as a result of geometrical constraints on the atom beam [25].

Since comparisons between laser cooling theories and experiments have centered on the velocity distribution and its spread, it might seem from the above discussion that a compar-

ison cannot be made when the angular distribution is measured. This is not so, however, because calculations can go one additional step to include the effects of correlation between transverse and longitudinal velocities and calculate an angular distribution. This should be relatively straightforward for a quantum Monte Carlo approach.

In the absence of a quantum Monte Carlo calculation applicable to our specific conditions, it is interesting to calculate the angular distribution that would result if steady-state conditions prevailed. With this assumption, there is no correlation between the velocities, and the angular distribution is given by

$$P(\alpha)d\alpha = \left[\int_0^\infty dv_z F(v_z\alpha)G(v_z)v_z \right] d\alpha, \quad (2)$$

where $\alpha \equiv v_x/v_z$ is the angle between the velocity vector and the beam axis, $F(v_x)dv_x$ is the (presumed known or calculated) transverse velocity distribution, and $G(v_z)$ is the thermal distribution given by $v_z^2 \exp(-v_z^2/2v_0^2)$, with $v_0^2 = k_B T/M$, k_B being the Boltzmann constant, M the atomic mass, and T the oven temperature. We note that $P(\alpha)$ is an atomic *density* angular distribution, as opposed to a *flux* distribution, so the thermal distribution $G(v_z)$ contains a factor of v_z^2 instead of the more familiar v_z^3 . The extra factor of v_z in eq. (2) comes from the relation $dv_x = v_z d\alpha$.

An analytical form for $P(\alpha)$ can be obtained if $F(v_x)$ is Gaussian, as it would be for low-excitation, steady-state conditions. With the RMS deviation of $F(v_x)$ defined to be v_{0x} , we obtain

$$P(\alpha)d\alpha = 2 \left(\frac{v_{0x}^2 v_0^2}{\alpha^2 v_0^2 + v_{0x}^2} \right)^2 d\alpha. \quad (3)$$

The squared-Lorentzian distribution of eq. (3) will be used below for comparing steady-state, low-excitation theory to our results.

III. EXPERIMENT

Fig. 1 shows our experimental arrangement, which includes the vacuum chamber with atomic beam source, the laser system for atomic beam collimation, and the fluorescence

probe and imaging system used to determine the angular distribution of the atoms on the beam axis.

Atomic beam

The chromium beam was produced using a radiatively heated tantalum crucible with a 1 mm circular aperture. Typical operating temperatures of 1550°C produce a most probable longitudinal velocity of $(2k_B T/M)^{1/2} = 761$ m/s. The longitudinal velocity distribution was measured and found to be in excellent agreement with a thermal distribution characterized by the crucible temperature. The beam was further defined with a 1 mm square aperture 450 mm from the crucible. The atomic beam was then cooled by 1-D optical molasses located 50 mm downstream from the square aperture. The 7S_3 to 7P_4 dipole transition was used for cooling, at a wavelength of $\lambda = 425.43$ nm (in air), with a linewidth of $\Gamma/2\pi = 5$ MHz and saturation intensity $I_0 = 8.5$ mW/cm². The initial angular distribution entering the molasses, determined by the 1 mm circular aperture of the crucible, had a base width of ≈ 2 mrad.

Naturally occurring Cr includes 83.8% ${}^{52}\text{Cr}$ which is free of hyperfine structure. The other isotopes were not cooled or detected in our experiments. Atoms pumped to the 7P_4 excited state can also decay to the ${}^5D_{3,4}$ metastable states, where they will remain trapped and undetectable using our fluorescence techniques. The branching ratio is approximately 1:5500, which implies approximately 8% loss for our interaction times. We assume that to first order the atoms are lost proportionally from all transverse velocity groups, and that this loss does not have a significant effect on the final angular distributions.

Laser

A single-mode ring-dye laser with stilbene-420 dye, pumped with 4 Watts of UV argon ion laser light, typically produced 200-300 milliwatts of blue light at 425.43 nm. The laser was

locked to the atomic transition using a split photodiode technique [26], calibrated against a saturable absorption cell.

The Gaussian laser beam was expanded asymmetrically using cylindrical lenses to a $1/e^2$ width of 23 ± 1 mm along the atom beam (Fig. 2a), and a $1/e^2$ width of 4.2 ± 0.2 mm transverse to the atom beam. This laser profile produced our best atomic beam collimation.

The laser beam profile used for our studies of intensity and detuning dependence was obtained by truncating the Gaussian beam along the atom beam symmetrically about the center to a length of 10.6 ± 0.5 mm. This produced a nominally uniform intensity that fell off by 27% at the ends of the interaction region (Fig. 2b), and dropped off by 11% at the edges of the atom beam.

The truncation of the laser beam was done at a distance of 175 mm from the atom beam, and as a result diffraction caused the truncated edge to fall off with a certain width. To determine whether this width had an effect on our results, for instance as might be caused by residual adiabatic cooling as the atoms exit the cooling region [22], we also performed tests with the truncation much closer to the atom beam, at a distance of 12.5 mm. The intensity fall-off (90%–10%) occurred in 0.24 mm for the 175 mm separation and 0.074 mm for the 12.5 mm separation. No significant difference was seen between data taken with the two truncation locations.

The effective laser intensity for the nominally uniform profile was obtained by fitting Gaussian functions to the full laser profiles along (see Fig. 2a) and transverse to the atom beam. The resulting two-dimensional Gaussian laser profile was normalized by setting the integral equal to the measured total power in the laser beam. The profile was then averaged over a 1 mm by 10 mm rectangle to give the effective intensity in the interaction region.

The laser cooling region was produced by retroreflecting the linearly polarized laser beam from a multilayer dielectric mirror and quarter-wave retarder combination located inside the vacuum chamber. Three orthogonal pairs of Helmholtz coils were used to bring the magnetic field in the interaction region to a level of $0 \pm 2\mu\text{T}$.

Angular distribution measurement

We determined the angular distribution in the atom beam after interaction with the laser cooling using a novel fluorescence imaging technique [27]. The atomic beam was partially blocked by a knife edge, located a distance $l = 120$ mm beyond the cooling region, and the atoms were then allowed to drift a distance $L = 660$ mm until they intersected a probe laser beam (see Fig. 1). The transverse spatial profile of the atomic beam, representing a shadow of the knife edge, was recorded by capturing an image of the fluorescence from the probe with a CCD camera; this profile was then used to obtain the angular distribution as follows.

We first assume that the angular distribution is the same for all locations at the exit of the cooling region over a spatial extent $\delta x = \Delta x l/L$, where Δx is the width of the transverse spatial profile at the probe. For all measurements, δx is no larger than 0.1 mm, or about 1/10th of the atom beam width, so this is a good assumption. We then relate the spatial profile at the probe to the angular distribution in the beam $f(\alpha)$ by

$$I(x) = \int_{\tan^{-1}(x/L)}^{\pi/2} f(\alpha) d\alpha, \quad (4)$$

where x is the distance along the profile and $x = 0$ is defined as the location where the knife edge cuts the atomic beam. The angular distribution is thus obtained by differentiating the spatial intensity profile and taking the limit $x/L \ll 1$ to yield

$$f(\alpha) = -L \frac{dI(x)}{dx}. \quad (5)$$

A typical spatial profile and derivative are shown in Fig. 3.

We note that the atomic beam is not perfectly uniform, as seen by the gentle curvature at the top of the profile in Fig. 3a, and this affects the derivative in a manner unrelated to the true angular distribution. This complication was avoided by using only the points in the shadow of the knife edge, i.e. where $x > 0$. To extract these points we applied a non-parametric smoother to the negative peak of the derivative, locating the local minimum, and mirrored the data for $x > 0$ about this point.

The imaging system on the CCD camera consisted of a 425 nm line filter and a 105 mm f/1.8 camera lens on a bellows extension. The captured two-dimensional image was band-averaged along the atom beam in the central, brightest portion of the fluorescence to yield the line scans such as the one shown in Fig. 3a. Calibration of the imaging system was carried out by capturing images of a calibrated scale, which showed that one pixel of the CCD camera corresponded to $8.8\ \mu\text{m}$ at the atom beam, or an angle of 0.013 mrad.

The probe laser was focused using a cylindrical lens to provide a thin plane of illumination, with thickness $\approx 200\ \mu\text{m}$, lying along the cooling direction and perpendicular to the imaging system. This reduced the depth of field required of the imaging optics. It also ensured measurement of only a small vertical (i.e. transverse) section of the beam for which the cooling laser intensity was approximately constant. The probe laser power was typically 5 mW, chosen to obtain sufficient fluorescence intensity without increasing the measured angular spread of the atomic beam (which occurs at higher power levels because saturation causes the effective thickness of the illumination plane to increase). It is worth noting that the Doppler shifts associated with the angular spreads found in this experiment are in the range of 0.3 MHz, far smaller than the natural linewidth of 5 MHz. Measuring the transverse velocities spectroscopically would therefore be extremely difficult.

Uncertainties in the angular distribution measurements were predominantly a result of noise in the profiles, with a minor contribution (1%) from uncertainty in the conversion from pixels to angle. The contribution of the noise to the derived quantiles was estimated by a “bootstrap” approach, in which (1) the profiles were smoothed until they appeared noise-free, (2) the standard deviation of the difference (residual) between the smoothed and raw data was calculated, (3) 1000 artificial data sets were generated by adding random numbers with the same standard deviation to the smoothed profile, (4) quantiles for each artificial data set were calculated, and (5) the standard deviation of these quantiles was calculated.

The angular distributions also include a contribution due to convolution with the edge resolution of the optics, which was measured by capturing the image of a sharp edge placed at the atom beam location. The derivative of this image had a 50% quantile of 0.013 mrad

and a 90% quantile of 0.026 mrad. No correction was performed to remove this contribution.

IV. RESULTS AND DISCUSSION

Fig. 4 shows the measured angular distribution for laser cooling with the full Gaussian laser beam profile shown in Fig. 2a. The single-beam laser power for this measurement was 40 mW and the detuning was $-\Gamma$. This distribution represents the highest degree of collimation observed, with 90% of the atoms within 0.61 ± 0.02 mrad and 50% within 0.16 ± 0.01 mrad.

Fig. 5 shows the complete set of measured distributions obtained using the truncated, nominally uniform laser profile, for various intensities and several detunings. Besides showing the distributions as a function of intensity for a range of detunings, we also display the effective light shift potential well depths U_0 for each measurement so that correspondence can be made with cooling theories. In determining U_0 for our data, there is some ambiguity as to the correct expression. Eq. (1) is strictly only valid for low excitation fraction, and our experiments are generally not carried out in this regime. If there is a significant excited state population, the overall effective potential is modified by the potentials of the excited state. To approximately take account of this we choose to calculate the average light shift of the ground state and the excited state weighted by their populations, given by [12,28]

$$U_0 = \frac{\hbar\Delta}{2} \ln \left(1 + \frac{4\Omega^2}{\Gamma^2 + 4\Delta^2} \right), \quad (6)$$

where in eq. (6) Ω is the Rabi frequency derived from the intensity in only one of the two laser beams making up the polarization gradient laser cooling region. While eq. (6) is strictly valid only for equilibrium conditions, we feel it gives a closer approximation to the true effective potential than eq. (1). We note that these two expressions become equivalent for low excitation fraction, i.e., in the limit of low intensity and/or large detuning.

At low light shifts the distributions shown in Fig. 5 have a semicircular shape with a small central peak. The semicircular part of this distribution consists of atoms that do not

have sufficient time to interact with the cooling laser. The shape is a direct consequence of the circular source aperture in the chromium oven. The small central peak represents the small, but increasing, fraction of atoms that are cooled. As only a small fraction of the atoms appear to be affected by the cooling, these distributions are most likely far from steady-state conditions.

At the higher light shifts the distributions appear to be completely modified by the cooling process, with the majority of the atoms cooled from the background into the narrow central peak. We expect that these distributions are the closest to steady-state conditions, since the shape is not unlike that predicted by eq. (3). However, even at the highest light shifts, there are small tails at large angles that could be either incompletely cooled atoms, or high-velocity components of a steady-state transverse velocity distribution.

To further quantify the distributions shown in Fig. 5, we have calculated 50% and 90% quantiles, α_{50} and α_{90} , of the distributions, which were determined by summing the data as a function of angle and examining the result. As mentioned above, the quantiles provide a simple, unbiased measure of the angular width of the distribution, and are useful experimental quantities if one wishes to know how much atomic flux can be passed through a given aperture size with a specific amount of cooling. We calculate both the 50% and 90% quantiles, as this gives more information about the overall shape of the distribution. For example, if the α_{50} remains small, but α_{90} increases, this indicates that the distribution is retaining a narrow peak, but is gaining wings.

Fig. 6 shows the quantiles derived from the distributions shown in Fig. 5. Both α_{50} and α_{90} are plotted as a function of U_0 , defined in eq. (6), for various detunings. Also shown for reference in Fig. 6 is the calculated excited state fraction f_{ex} for the strongest ($|M| = J \rightarrow |M| = J + 1$) transition, given by

$$f_{\text{ex}} = \frac{\Omega^2}{\Gamma^2 + 2\Omega^2 + 4\Delta^2}. \quad (7)$$

All the quantiles shown in Fig. 6 have similar behavior for lower values of U_0 , decreasing as U_0 is increased until a minimum is reached around $U_0 \approx 100E_r$. This initial decrease

is consistent with an approach toward steady-state conditions, with more and more atoms being captured by the cooling process. The shapes of the distributions in Fig. 5 bear this out, showing a disappearance of the uncooled, semicircular distribution. The variation with detuning is also in accord with this picture, as one would expect steady-state conditions to require higher values of U_0 for larger detunings.

After reaching a minimum, the quantiles increase slowly as U_0 is increased further, with larger detunings increasing more slowly than smaller ones. This increase is a result of heating from spontaneous emission, which competes with the cooling processes. The faster increase for smaller detunings is clarified by considering the excited state fraction, which is much larger for the smaller detunings.

Also shown in Fig. 6 are the results of a low-excitation, steady-state one-dimensional calculation [16]. The calculation predicts the transverse average kinetic energy for laser cooling of rubidium, which has a cooling transition with the same angular momenta as chromium ($J = 3 \rightarrow J = 4$). The results should be directly applicable to chromium, provided everything is scaled by the recoil energy E_r . The calculated kinetic energies were transformed into angular distributions using eq. (3), which assumes a Gaussian transverse velocity distribution and no correlation between longitudinal and transverse velocities, consistent with steady-state, low-excitation conditions. The angular distributions were then integrated numerically to obtain the quantiles.

The agreement between the theory and experiment is remarkable for α_{50} , considering the disparity in conditions. While an expected divergence is seen at low values of U_0 , due to the uncaptured portion of the atom beam, the agreement is quite good for larger values of U_0 . Particularly good agreement is seen for the larger detunings, which is perhaps understandable because these have the smallest excited-state fraction.

The experimental values for α_{90} lie consistently higher than those calculated. A likely cause of this situation is a difference between the shapes of the experimental and theoretical angular distributions, since if the shapes were the same, both quantiles would have to agree equally well. That α_{90} is larger than the theory indicates that the distribution has large-

angle tails, which is consistent with the type of non-Gaussian velocity distribution observed in high-excitation cooling calculations [23,24]. An even larger difference is seen between theory and experiment for smaller detunings, which again points toward a strong effect due to a high excitation fraction.

While the agreements and disagreements between the experiment and low-excitation, steady-state theory are interesting, a few caveats must be kept in mind before too many conclusions are drawn. First, the general decrease in α_{50} and α_{90} at small values of U_0 for both the theory and experiment probably arises from very different effects: the experiment decreases because more and more atoms are participating in the cooling process, while the theory (which always assumes all atoms participate fully) decreases because of increased cooling efficiency. Second, the role of correlation between the longitudinal and transverse velocities may have significant effects, yet is not really considered in this comparison. Third, there is still some ambiguity in the choice of definition for U_0 . It is somewhat unsatisfactory that the definitions are different for the theory and experiment, yet it is clearly inappropriate to use a low-excitation definition for our experimental conditions.

V. SUMMARY

These experiments have shown that a chromium beam can be transversely cooled and collimated well below the Doppler limit using (*lin* \perp *lin*) molasses. Using a Gaussian laser profile, 50% of the beam can be collimated within 0.16 ± 0.01 mrad. Applications which require intense and well-collimated atomic beams, such as atomic interferometry [1], collisional studies [3], and nanofabrication using atom optics [4], can benefit from these results which demonstrate that a large number of atoms in a beam can be collimated efficiently, to an angular width corresponding to a few times the recoil velocity, in a short interaction time.

The conventional models of laser-atom cooling, based on assumptions of infinite interaction times and low excited state fractions, are clearly not applicable to the cooling of

atoms over a limited interaction distance in a thermal beam. Interestingly, however, our measurements show the general trends expected from low-excitation approaches, which predict improved cooling and reduced kinetic energies along the laser axes as the light shift is increased from zero, reaching a characteristic minimum energy spread before rising due to diffusion heating effects at higher laser intensities.

The particular shape of the angular distributions has not previously been considered, and yet this is of essential importance to the application of laser cooling for the production of collimated atomic beams. The distribution is of particular interest for non-equilibrium conditions, where the contribution of the large-angle wings to the total transverse kinetic energy can be quite large, even while the bulk of the atomic beam is well collimated.

To further experimentally explore one-dimensional laser cooling in an atomic beam, use of a velocity-selected atomic beam or velocity-selective detection would be highly desirable. This would not only permit measurement of beam collimation for well-defined interaction times, but also allow direct measurement of the transverse velocity distribution.

To learn more about the cooling processes underlying the collimation of a thermal atomic beam, much insight could be gained by carrying out time-dependent quantum Monte-Carlo calculations for conditions corresponding to the present work, and deriving angular distributions taking into account all velocity correlations and non-steady-state effects.

We are indebted to T. Bergeman and P. Marte for many invaluable discussions and theoretical calculations, and would also like to thank M. D. Stiles, W. D. Phillips and S. Rolston for their advice and suggestions. This work was supported in part by NSF Grant No. PHY-9312572 and by the Technology Administration of the U. S. Department of Commerce.

REFERENCES

- * Present address: School of Physics, University of Melbourne, Parkville Vic 3052, Australia.
- [1] See special issue Appl. Phys. B **54**, 321 (1992), and C. S. Adams, M. Sigel and J. Mlynek, Phys. Rep. **240**, 143 (1994).
- [2] J. Vanier and C. Audoin, *Quantum Physics of Atomic Frequency Standards* (Adam Higler, Bristol, 1989).
- [3] M. Jacka, J. Kelly, B. Lohmann, and S. Buckman, Australian J. Phys., **49**, 515 (1996).
- [4] G. Timp, R. E. Behringer, D. M. Tennant, J. E. Cunningham, M. Prentiss and K. K. Berggren, Phys. Rev. Lett. **69**, 1636 (1992), J. J. McClelland, R. E. Scholten, E. C. Palm and R. J. Celotta, Science **262**, 877 (1993), R. E. Scholten, J. J. McClelland, E. C. Palm, A. Gavrin, and R. J. Celotta, J. Vac. Sci. Technol. B **12** 1847 (1994).
- [5] J. A. Giordmaine and T. C. Wang, J. Appl. Phys. **31**, 463 (1960).
- [6] N. Ramsey, *Molecular Beams*, (Clarendon Press, Oxford, 1956).
- [7] C. E. Tanner, B. P. Masterson, and C. E. Weiman, Opt. Lett. **13**, 357 (1988).
- [8] B. Sheehy, S.-Q. Shang, P. van der Straten and H. Metcalf, Chem. Phys. **145** 317 (1990).
- [9] M. D. Hoogerland, J. P. J. Driessen, E. J. D. Vredenburg, H. J. L. Megens, M. P. Schuwer, H. C. W. Beijerinck, and K. A. H. van Leeuwen, Applied Physics B **62**, 323 (1996).
- [10] S. V. Andreev, V. I. Balykin, V. S. Letokhov, and V. G. Minogin, JETP Lett. **34**, 463 (1981); W. D. Phillips and H. Metcalf, Phys. Rev. Lett. **48**, 596 (1982); S. Chu, L. Holberg, J. E. Bjorkholm, A. Cable, and A. Ashkin, Phys. Rev. Lett. **55**, 48 (1985).
- [11] See special issues, *The Mechanical Effects of Light*, J. Opt. Soc. Am. B **2**, 1706 (1985) and *Laser Cooling and Trapping of Atoms*, J. Opt. Soc. Am. B **6**, 2020 (1989).

- [12] J. Dalibard and C. Cohen-Tannoudji, *J. Opt. Soc. Am. B* **6**, 2023 (1989).
- [13] P. J. Ungar, D. S. Reiss, E. Riis, and S. Chu, *J. Opt. Soc. Am. B* **6**, 2058 (1989).
- [14] Y. Castin and J. Dalibard, *Europhys. Lett.* **14** 761–766 (1991); Y. Castin, J. Dalibard, and C. Cohen-Tannoudji, in *Light Induced Kinetic Effects on Atoms, Ions and Molecules*, edited by L. Moi, S. Gozzini, C. Gabbanini, E. Arimondo, and F. Strumia, (ETS Editrice, Pisa, 1991), p. 5 (1991)
- [15] T. Bergeman, *Phys. Rev. A* **48**, R3425 (1993).
- [16] P. Marte, R. Dum, R. Taïeb, P. D. Lett, and P. Zoller, *Phys. Rev. Lett.* **71** 1335 (1993).
- [17] P. D. Lett, W. D. Phillips, S. L. Rolston, C. E. Tanner, R. N. Watts, and C. I. Westbrook, *J. Opt. Soc. Am. B* **6**, 2084 (1989).
- [18] C. Gerz, T. W. Hodapp, P. Jessen, K. M. Jones, W. D. Phillips, C. I. Westbrook, and K. Molmer, *Europhys. Lett.* **21**, 661 (1993).
- [19] C. Salomon, J. Dalibard, W. D. Phillips, A. Clarion, and S. Guellati, *Europhys. Lett.* **12** 683 (1990).
- [20] P. S. Jessen, C. Gerz, P. D. Lett, W. D. Phillips, S. L. Rolston, R. J. C. Spreeuw and C. I. Westbrook, *Phys. Rev. Lett.* **69** 49 (1992).
- [21] Uncertainty estimates quoted in this paper are to be interpreted as one standard deviation combined random and systematic uncertainties unless otherwise indicated.
- [22] J. Chen, J. G. Story, J. J. Tollett and R. G. Hulet, *Phys. Rev. Lett.* **69** 1344 (1992).
- [23] P. Marte, private communication
- [24] T. Bergeman, private communication.
- [25] While the longitudinal and transverse velocity distributions of a thermal atom beam are completely uncorrelated if one considers only the velocity distributions integrated over

all spatial variables, correlation is introduced if one asks what the velocity distributions are at a specific point in space, or if one spatially limits the beam such as by placing an aperture in it. This is illustrated by considering a thermal beam emerging from an infinitesimal pinhole. Examining the velocity distributions at an angle α from the axis of the pinhole, one finds that all the atoms have a transverse-to-longitudinal velocity ratio $\tan \alpha$. If an aperture that subtends an angle α is placed in the beam, atoms of a given longitudinal velocity v_z can only have transverse velocities with magnitude $\leq v_z \tan \alpha$. Thus the velocity distributions are correlated. This correlation is an important consideration when relating an angular distribution to transverse and longitudinal velocity distributions.

[26] J. J. McClelland and M. H. Kelley, Phys. Rev. A **31** 3704 (1985).

[27] Measurements were also made in which a narrow slit was placed in front of the interaction region and the spatial distribution of the atomic beam was imaged. Comparable results were obtained with this geometry.

[28] J. P. Gordon and A. Ashkin, Phys. Rev. A **21**, 1606 (1980).

FIGURES

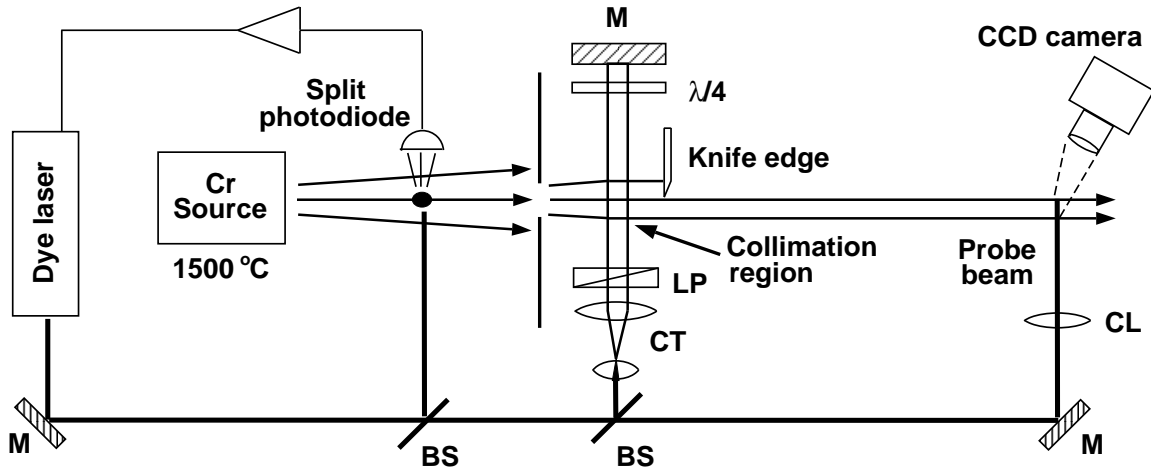


FIG. 1. Experimental arrangement, showing effusive chromium source (at 1550 °C) with 1 mm diameter aperture, split photodiode for frequency locking, precollimating aperture (1 mm × 1 mm), molasses region, knife edge and fluorescence imaging detector. The optical elements shown are mirror (M), beamsplitter (BS), linear polarizer (LP), cylindrical telescope (CT), cylindrical lens (CL) and quarter-wave retarder ($\lambda/4$).

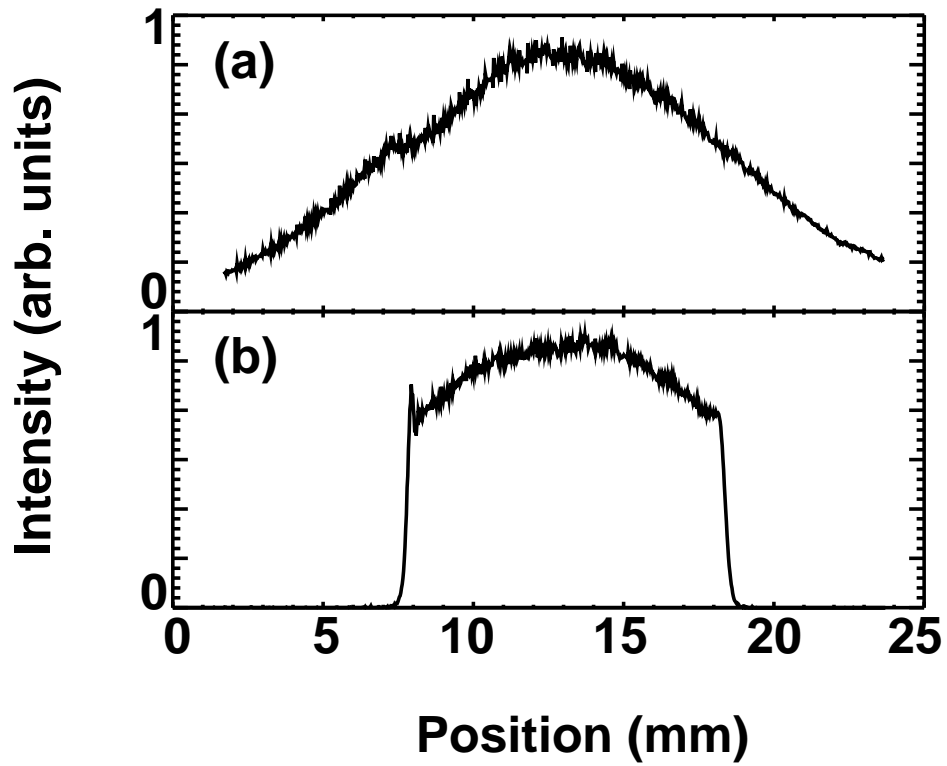


FIG. 2. Laser intensity profiles along the direction of the atom beam, measured at the interaction region: (a) full Gaussian profile and (b) truncated profile. A fit to the Gaussian profile yields a $1/e^2$ full width of 23 ± 1 mm. The truncated profile has a full-width at half-maximum of 10.6 ± 0.5 mm. The laser profile perpendicular to the atom beam (not shown) was very nearly Gaussian with $1/e^2$ full width of 4.2 ± 0.2 mm.

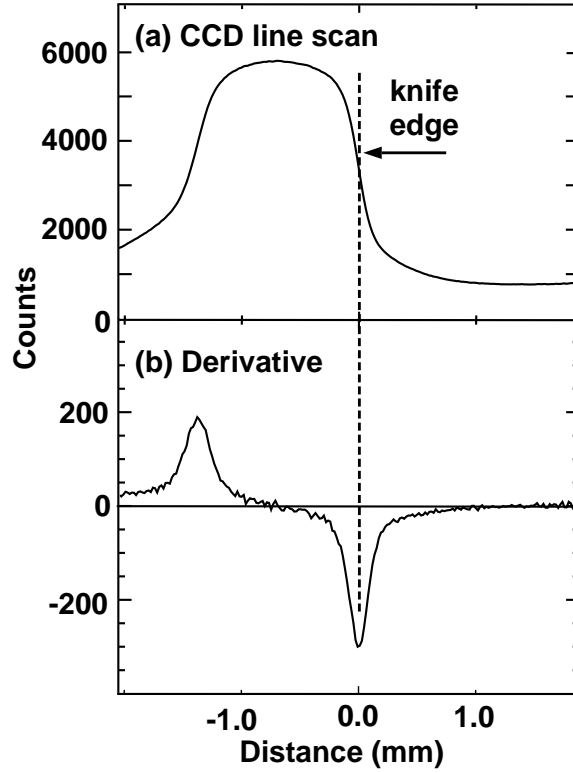


FIG. 3. Fluorescence profiles of the atomic beam acquired by capturing an image with the CCD imaging camera and band-averaging along the direction of the atom beam. (a) Transverse profile of a laser-collimated atomic beam, showing knife edge shadow. (b) Spatial derivative of the profile shown in (a).

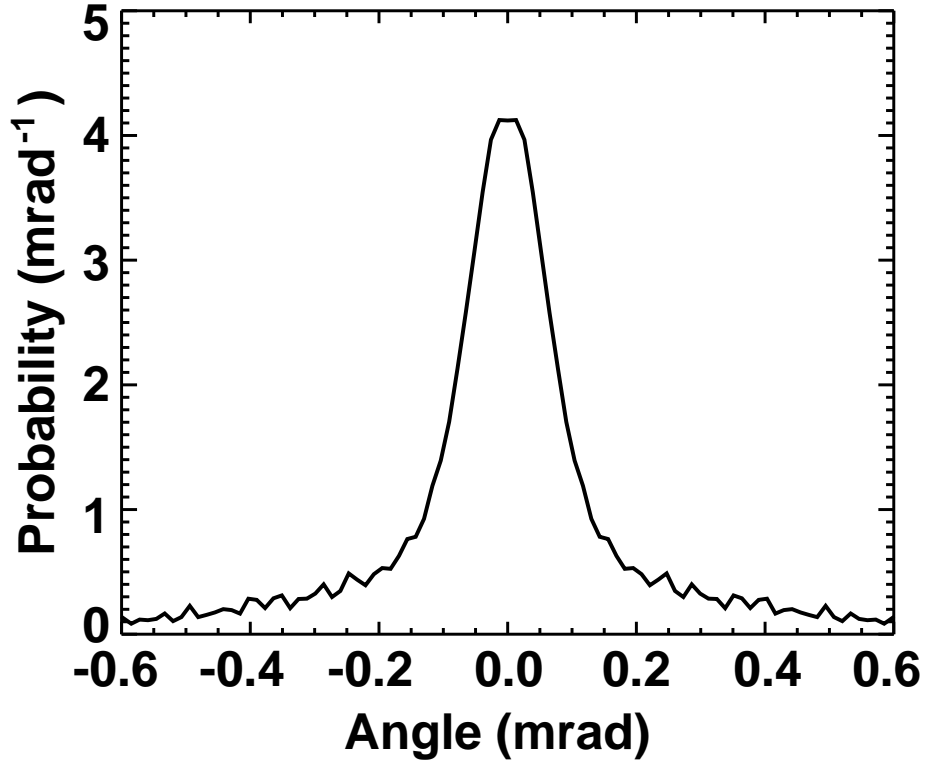


FIG. 4. Angular distribution of the cooled Cr beam obtained by inverting and symmetrizing a derivative profile such as shown in Fig. 3b. This distribution corresponds to the highest degree of collimation observed, obtained by using a Gaussian laser beam (Fig. 2a) with total power 40 mW and detuning $-\Gamma$. 90% of the atoms are within 0.61 ± 0.02 mrad and 50% are within 0.16 ± 0.01 mrad.

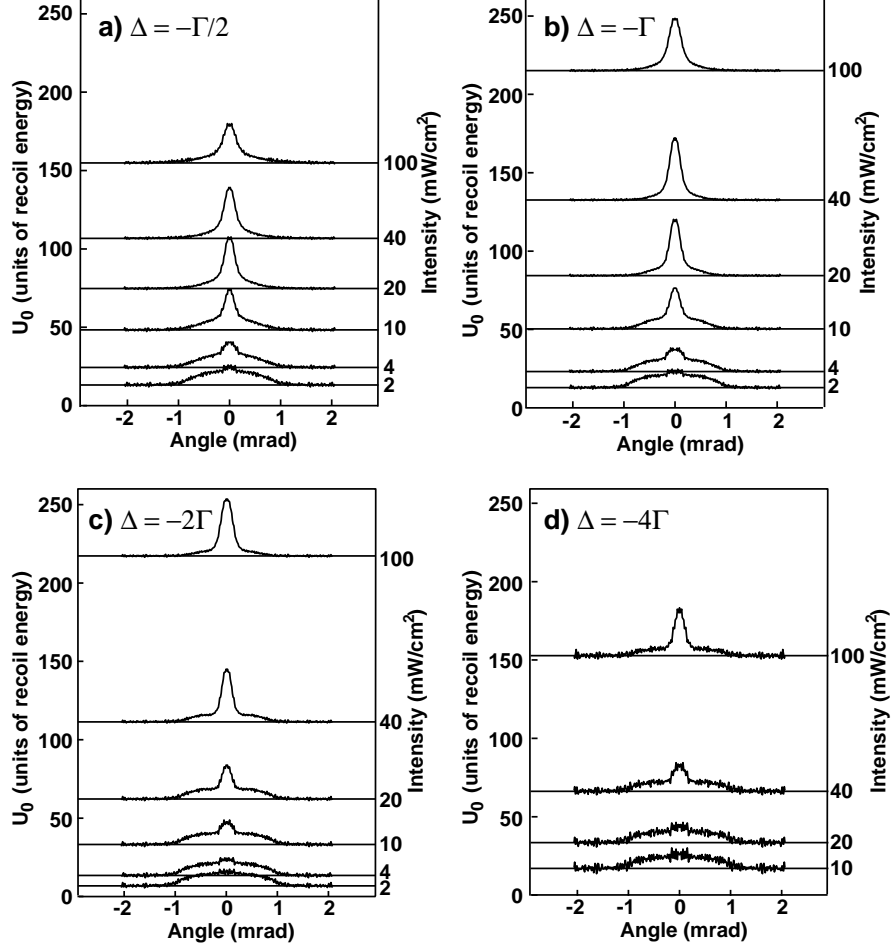


FIG. 5. Angular distributions of the cooled Cr beam obtained by inverting and symmetrizing derivative profiles such as shown in Fig. 3b, displayed as a function of laser detuning Δ and intensity. (a) $\Delta = -\Gamma/2$, (b) $\Delta = -\Gamma$, (c) $\Delta = -2\Gamma$, and (d) $\Delta = -4\Gamma$, where Γ is the natural linewidth of Cr ($2\pi \times 5$ MHz). The profiles are plotted in such a way as to also display for each case the effective potential well depth U_0 , given by eq. (6), and also the corresponding laser intensity. Each profile is given a vertical offset corresponding to its value of U_0 , and the scale is given on the left vertical axis of each plot. The scale for the intensity is given on the right vertical axis. The profiles are all normalized to have unity area.

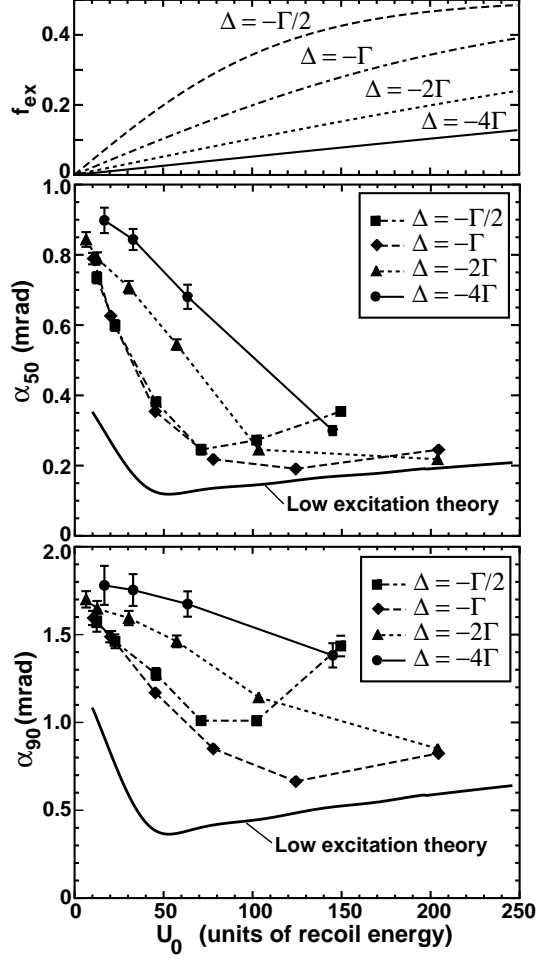


FIG. 6. Angular quantiles for the angular distributions shown in Fig. 5, plotted as a function of the effective potential well depth U_0 , given by eq. (6). These quantities are defined as the angular width that encompasses a specific integrated fraction of the profile. (a) 50% quantile, (b) 90% quantile. Different detunings Δ are indicated by different plotting symbols and line types, as shown in the inset. Uncertainties are one standard deviation, and are shown only where larger than the plotting symbol. A calculation of the quantiles based on a low-excitation, equilibrium theory is also indicated in each graph by the heavy solid curve. Also shown for reference at the top of the figure is the calculated excited state fraction f_{ex} (eq. 7) for the different detunings.